Atmospheric correction algorithm of visible and near-infrared satellite data using radiance components: pixel-by-pixel calculation of the adjacency effect

Mitsuo Minomura, Hiroaki Kuze, and Nobuo Takeuchi
Center for Environmental Remote Sensing (CEReS),
Chiba University, 1-33, Yayoi-cho, Inage-ku, Chiba, 263-8522, Japan
mino@ceres.cr.chiba-u.ac.jp

Key words: atmospheric crrection, radiance components, adjacency effect, aerosol extinction profile, single scattering, optical thickness, radiative transfer

1. Introduction

In this paper we describe the framework of an atmospheric correction algorithm which we have developed recently. The algorithm is for the correction of visible and near-infrared satellite images, with ancillary information on atmospheric parameters obtained with a sun photometer and a multi-wavelength lidar. The ground observations synchronized with the satellite overpass provide the aerosol optical thickness τ_a, its wavelength dependence, and the vertical profile of the aerosol extinction coefficient. In the algorithm, first the pixel reflectance is analytically expressed in terms of radiance components detected by a satellite sensor. This scheme enables us to calculate the influence of the atmospheric extinction using a general radiative transfer code such as the MODTRAN3. The second part of the algorithm deals with the range ($N \times N$ pixels around the target) in which the adjacency effect should be incorporated. We assume that the optical thickness τ_a is relatively small, hence the scattering process is reasonably handled by the single scattering approximation. Simulation results indicate that both τ_a and aerosol vertical distribution play significant role in the determination of τ_a.

In Sec. 2, we describe the essential aspects of the present algorithm for the atmospheric correction. The accuracy of the retrieval of ground reflectance is also discussed. In Sec. 3, the basic concept of the single scattering treatment of the adjacency effect evaluation is presented along with simulation results.

2. Atmosphric correction

2.1 Algorithm

Our algorithm[1] is based on Richter's two-step algorithm[2]. If we assume in his algorithm that a responce function takes a constant value within the sensor bandwidth, the equation of the first-order reflectance, $\rho^{(1)}$, can be simplified as follows

$$\rho^{(1)} = \rho_{\mathrm{MOD}} \frac{L_{\mathrm{pix}} - L_0}{L_{\mathrm{total}} - L_0} \qquad (1)$$

Here, ρ_{MOD} is the surface reflectance used in the MODTRAN calculation, L_{pix} is the pixel radiance observed by the sensor, and L_{total} and L_0, respectively, are the total and path radiances at the TOA obtained from the MODTRAN calculation. Figure 1(a) shows the dependence of MODTRAN radiance components on the surface reflectance. As can be seen from this figure, the value of $L_{\mathrm{total}} - L_0$ is proportional to the surface reflectance to a good approximation. This indicates that in Eq. (1) the ratio of $\rho_{\mathrm{MOD}}/(L_{\mathrm{total}} - L_0)$ does not depend on the value of ρ_{MOD} assumed in the MODTRAN calculation: in the present simulation, we use $\rho_{\mathrm{MOD}} = 0.2$.

The second-order expression of the adjacency effect correction becomes

$$\rho^{(2)} = \rho^{(1)} + \frac{L_{\mathrm{p}} - L_0}{L_{\mathrm{g}}} \left(\rho^{(1)} - \bar{\rho}^{(1)} \right) \qquad (2)$$

where $\bar{\rho}^{(1)} = \sum_{j=1}^{N^2} \rho_j^{(1)} / N^2$, L_{g} is the TOA radiance due to the ground reflection, and L_{p} is the path radiance: these are also obtainable through

the usual MODTRAN calculation, as given in Fig. 1(a).

Now, we consider improvement of the correction of the adjacency effect. In order to consider this effect, here we use the following expression, similar to Eq. (2), to define $\rho^{(3)}$:

$$\rho^{(3)} = \rho^{(2)} + \frac{L_p - L_0}{L_g}\left(\bar{\rho}^{(1)} - \bar{\rho}^{(2)}\right) \qquad (3)$$

Repeated application of similar procedure leads to an expression for k-th order correction of the adjacency effect:

$$\rho^{(k)} = \rho^{(k-1)} + \frac{L_p - L_0}{L_g}\left(\bar{\rho}^{(k-2)} - \bar{\rho}^{(k-1)}\right) \qquad (4)$$
$$k = 3, 4, \cdots$$

Tests have shown that usually the progression of $\rho^{(k)}$ converges for $k \geq 3$, and $k = 3$ gives sufficient accuracy. Here we use $\rho^{(3)}$ as the final form of the atmospheric correction. Thus, we have derived a three-step algorithm based on Eqs. (1), (2), and (3).

2.2 Validation method of the three-step algorithm

The MODTRAN code gives the TOA total radiance in a form of

$$L_{\text{total}} = L_{\text{gd}} + L_{\text{gi}_1} + L_{\text{gi}_2} + L_{\text{ps}} + L_{\text{pm}_1} + L_{\text{pm}_2} \quad (5)$$

where L_{gd} is the directly ground-reflected radiance, L_{gi_i} the indirectly ground-reflected radiance, L_{ps} the path radiance due to single scattering, and L_{pm_i} the path radiance due to multiple scattering. A detailed analysis shows that among these components, L_{pm_2} is proportional to the ground reflectance and L_{gi_2} is proportional to the square of the surface reflectance (Fig. 1(b)). Thus the total radiance that would be observed by a satellite sensor for a target pixel, then, can be expressed as

$$L_{\text{pix}} = L_{\text{gd}}(\rho) + L_{\text{gi}_1}(\rho) + L_{\text{gi}_2}(\rho, \bar{\rho}) + L_{\text{ps}} + L_{\text{pm}_1} + L_{\text{pm}_2}(\bar{\rho}) \qquad (6)$$

Here ρ is the target reflectance and $\bar{\rho}$ is the average reflectance. In the calculation of L_{pix} using Eq. (6), the reflectance dependence of each radiance component is determined by atmospheric conditions, the optical thickness at 550 nm, τ_{550},

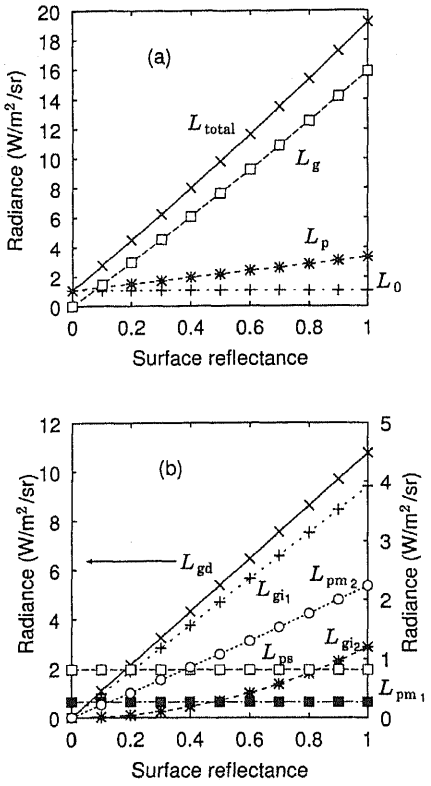

Figure 1: Surface reflectance dependence of the radiance components calculated for an aerosol optical thickness of 0.198. (a) Four radiance components in the MODTRAN code. (b) Each of L_{pm} and L_{gi} are separated into two components. The left ordinate is for L_{gd}, and the right ordinate is for the other five components.

and the aerosol model specified for the MODTRAN calculation (The aerosol model determines the wavelength dependence of the aerosol extinction). In the present simulation, we use the urban aerosol model.

The process of the present simulation is schematically shown in Fig. 2. The result is evaluated for the second- and third-step reflectances, $\rho^{(j)}$ $(j = 2, 3)$, by means of relative errors defined as $r^{(j)} = (\rho^{(j)} - \rho_t)/\rho_t$.

Since for each pixel, the relative importance of the adjacency effect differs in accordance with the pixel reflectance, we make a statistical consideration for each pixel group that consists of pixels characterized by the same reflectance. We define

Table 1: NOAA AVHRR data and related parameters. τ_{550} is the aerosol optical thickness at 550 nm derived from the simultaneous observation using a sunphotometer. S_j and I_j are the calibration (slope and intercept) constants for the channel j(=1,2) NOAA data.

No.	Date	Time	τ_{550}	S_1	I_1	S_2	I_2
1	1997/12/05	13:51	0.198	0.1338	-5.4876	0.1690	-6.9267
2	1998/12/28	14:22	0.317	0.1304	-5.3464	0.1531	-6.2776
3	1999/04/14	14:32	0.357	0.1321	-5.4172	0.1548	-6.3474
4	1999/07/29	14:46	0.150	0.1336	-5.4762	0.1562	-6.4055

the average value of the relative error $r^{(j)}$ as

$$\bar{r}^{(j)}(\rho_t) = \sum_{\rho_t} r_i^{(j)}/m(\rho_t) \qquad (7)$$

where the summation is carried out for $m(\rho_t)$ pixels which has the original reflectance of ρ_t. Similarly, we define the standard deviation of $r^{(j)}$ as

$$\sigma^{(j)}(\rho_t) = \left[\frac{1}{m(\rho_t)-1}\sum_{\rho_t}\left(r_i^{(j)} - \bar{r}^{(j)}(\rho_t)\right)^2\right]^{1/2} \qquad (8)$$

If the atmospheric correction of the $L_{\rm pix}$ image were carried out in a perfect way, both $\bar{r}^{(j)}(\rho_t)$ and $\sigma^{(j)}(\rho_t)$ become zero.

2.3 Sensitivity analysis using the AVHRR data

2.3.1 AVHRR data

Table 1 shows the NOAA14 AVHRR data used in the present simulation and analysis. The satellite overflight took place between 1:30 and 3:00 p.m. over the Chiba area: each image (190×190 pixels) was taken at the near nadir angle centered at the area. Both channel 1 and channel 2 images are employed here.

For each satellite data in Table 1, we use the aerosol optical thickness obtained using a sunphotometer at the time of the NOAA14 overflight. The value at 550 nm, τ_{550}, which is required as an input parameter in the MODTRAN calculation, is determined by the interpolation of the eight-wavelength sunphotometer data. The values are listed in the fourth column of the table.

For the other parameters given to the MODTRAN code, we employ the standard atmosphere (midlatitude) and the urban aerosol model for the wavelength dependence of the aerosol extinction.

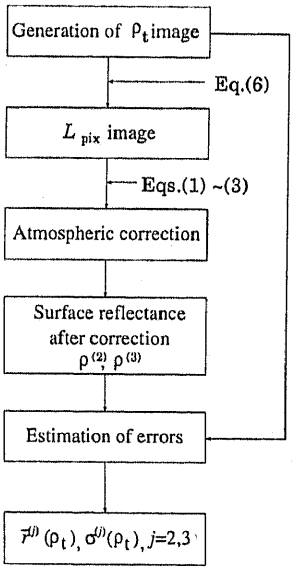

Figure 2: Flow chart of the sensitivity analysis of the present three-step atmospheric correction algorithm.

The wavenumber region is 14184 ~ 17467 cm^{-1} for channel 1 and 9975 ~ 13840 cm^{-1} for channel 2. Both the bin width and the width of the triangular function are taken to be 40 cm^{-1}. This corresponds to the assumption of the uniform sensitivity over the sensor bandwidth in the calculation of the radiance components.

2.3.2 Images for simulation

For the implementation of the method described in Sec. 2.2, we prepare images around the Chiba area based on the real satellite data after the atmospheric correction. The pixels with $\rho_t > 0.5$ are regarded as having $\rho_t = 0.5$. The size of the Chiba images is 186 × 186. We choose im-

ages No.2 and No.3 with relatively large values of the optical thickness to construct the test images.

In the MODTRAN calculation using eq. (6), we use the optical thickness at 550 nm (τ_{550}) in Table 1. For the calculation of the average reflectance $\bar{\rho}$, we study two cases of $N = 15$. It is noted that in the practical application of atmospheric correction, the choice of the range parameter N is crucial for the exact removal of the adjacency effect[3,4].

2.3 Retrieval with the same range parameter

We consider the case in which the same value of the range parameter is used for the preparation of the test image ($N_{\rm sim}$) and for the atmospheric correction ($N_{\rm ac}$).

The results are shown in Fig. 3: (a) is for the AVHRR channel 1 and (b) is for channel 2 of the image No.2 (December 28, 1998) and (c) channel 1 and (d) channel 2 of the image No.3 (April 14,1999). The step of the reflectivity, $\Delta\rho_{\rm t}$, is about 0.01. Improvement in the third-step result is evident as compared with the second-step one. For the pixel reflectance of less than $\sim$ 0.2, the retrieved pixel reflectance has an accuracy better than 1 % for channel 1 and 0.5 % for channel 2. In the case of the image No. 3, the relative error increases with $\rho_{\rm t}$. This is ascribed to the cloud pixels which are relatively small in number (less than 20 pixel for each reflectivity) yet quite influential to the neighboring pixels.

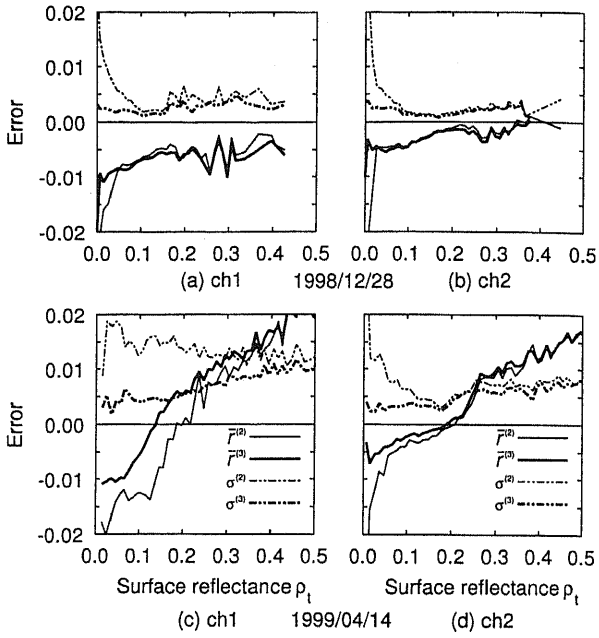

Figure 3: Retrieval errors for the Chiba images. (a) (AVHRR channel 1) and (b) (channel 2) are for the image No.2 (December 28, 1998), and (c) (channel 1) and (d) (channel 2) are for the image No.3 (April 14,1999). Pixel reflectances are retrieved with an accuracy of about 1 % (channel 1) and 0.5 % (channel 2) for pixels with relatively low reflectance of less than 0.2. Range parameter $N = 15$ is used for all cases.

3 Adjacency effect

3.1 Radiation component relevant to the adjacency effect

In the visible and near-infrared region of the solar spectrum, the purpose of the atmospheric correction is to extract the directly ground-reflected component $L_{\rm gd}$ from the six components depicted in Fig. 4. In the following, we evaluate the magnitude of the adjacency component corresponding to $L_{\rm pm_2}$ in Fig. 4. As compared with this term, other adjacency component, $L_{\rm gi_2}$, exhibits smaller contribution due to increase in the number of scattering processes involved.

Figure 5 illustrates the present configuration used to calculate the irradiance related to the adjacency effect. We assume that the atmosphere is horizontally layered, with a uniform extinction coefficient in each layer. The ground surface is planar and shows Lambertian reflection, with the reflectivity changing on a pixel by pixel basis. The photon relevant to $L_{\rm pm_2}$ is first reflected by an adjacent pixel, then scattered only once in the instantaneous FOV of the sensor element. In the following, for simplicity, μ stands for $\cos\theta$, with subscripts s, r, and v indicating the solar zenith angle, reflection angle, and observation angle, respectively. When the solar irradiance at the TOA is written as $E_{\rm ext}$, and the optical thickness from the ground to the TOA as $\tau_{\rm TOA}$, the downward solar irradiance at the ground is given as $E_{\rm g} = \mu_{\rm s} E_{\rm ext} e^{-\tau_{\rm TOA}/\mu_{\rm s}}$. It should be noted that for $E_{\rm g}$, we consider only the directly transmitted light. The scatterer (aerosol or molecule) is located at an altitude of z. The energy incident on the cross section σ of the scatterer per unit time

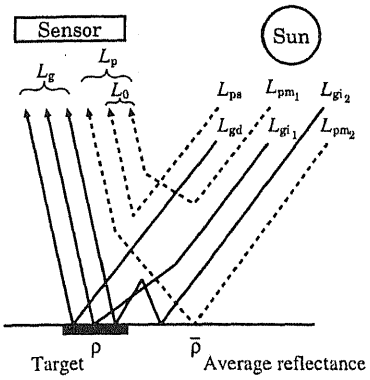

Figure 4: Radiance components detected by a satellite sensor. $L_{\rm gd}$: ground-reflected radiance, $L_{\rm p}$: path radiance, and L_0: dark target radiance.

is given by

$$\sigma E_{\rm in}(z,\mu_{\rm r}) = \mu_{\rm r}\frac{\rho\sigma E_{\rm g}A}{\pi r^2}e^{-\tau(z)/\mu_{\rm r}}. \qquad (9)$$

Here, A is the surface area of a pixel, ρ its reflectance, r the length of a vector connecting the reflecting pixel to the scatterer, $\theta_{\rm r}$ the zenith angle of $\mathbf{r}$, and $\tau(z)$ the optical thickness at the altitude z.

Next we consider the radiation flux $d\Phi_{\rm sp}(z)$ that is received by a single element (area dS_1) of the sensor located at a distance of R:

$$\frac{d\Phi_{\rm sp}(z)}{dS_1} = E_{\rm in}(z,\mu_{\rm r})\frac{\sigma}{R^2}p(\cos\Theta)e^{-\tau'(z)/\mu_{\rm v}}. \qquad (10)$$

Here Θ is the scattering angle, $p(\cos\Theta)$ is the phase function, and $\tau'(z)$ is the optical thickness from the particle to the sensor. Thus, eq. (10) describes the irradiance into the sensor element originating from the light that has reflected from the surface and then scattered by a single scatterer. It is also noted that the sensor element is the one relevant to the target pixel in the instantaneous FOV of the sensor.

The number of scattering particles $N(z)$ in an volume element dV is given by $N(z) = n(z)dV$, where $n(z)$ is the number density of scattering particles. The volume element can also be expressed as $dS(z)dz$, where $dS(z)$ is the base area of the volume element (see Fig. 5). Using the single scattering albedo ω_0 and the extinction coefficient $\alpha(z)$, the total scattering cross section

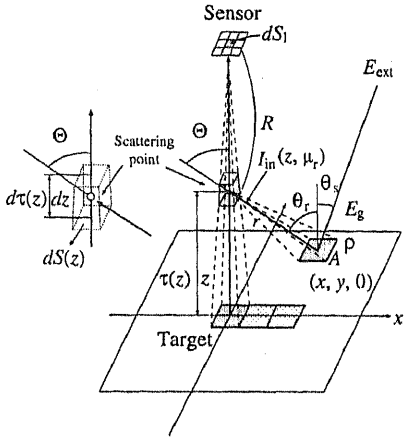

Figure 5: Calculation of the irradiance $E_{\rm adj}$ due to the adjacency effect. After reflected from an adjacent pixel located at $(x,y,0)$, the light ungdergoes a single scattering at $(0,0,z)$.

due to the particles inside dV is given as

$$\begin{aligned}\sigma N(z) &= \sigma n(z)dV \\ &= \omega_0\alpha(z)dS(z)dz. \qquad (11)\end{aligned}$$

Under this situation, the radiation flux to the sensor element from the volume element dV becomes

$$\frac{d\Phi_{\rm s}(z)}{dS_1} = E_{\rm in}(z,\mu_{\rm r})\frac{\omega_0\alpha(z)dS(z)dz}{R^2}\cdot p(\cos\Theta)e^{-\tau'(z)/\mu_{\rm v}}. \qquad (12)$$

In the actual evaluation, one has to consider contributions from both aerosol particles and molecules.

We take the origin of the coordinate system at the location of the target pixel. The total contribution from the light reflected at a pixel at $(x,y,0)$ is calculated by summing up contributions from all the atmospheric layers. Therefore, when l-fold layers are assumed, the irradiance due to the adjacency effect from that pixel is given by

$$E_{\rm s}(x,y) = \sum_{i=1}^{l}\frac{d\Phi_{\rm s}(z_i)|_{(x,y)}}{dS_1}. \qquad (13)$$

Since the total irradiance $E_{\rm adj}$ is obtained from a summation of $E_{\rm s}(x,y)$ over a sufficient number of pixels around the target, we have

$$E_{\rm adj} = \sum_{y=-n}^{n}\sum_{x=-n}^{n}E_{\rm s}(x,y), \qquad (14)$$

where n denotes a sufficiently large positive number: we consider $N \times N$ pixels ($N = 2n + 1$) in the computation of the adjacency effect. The basic features of the adjacency effect are determined by eqs. (12)–(14). Particularly, $E_s(x, y)$ in eq. (13) is an important quantity in that it gives the contribution of a single pixel located at $(x, y, 0)$, regardless of the reflectance values of other pixels. Below, unless otherwise noted, we use the effective reflectivity ρ that is obtained by normalizing E_{adj} to the downward solar irradiance E_{ext} at the TOA.

3.2 Optical Parameters

The composite values of the extinction coefficient $\alpha(z)$, phase function $p(\cos\Theta)$, and single scattering albedo ω_0, are given, respectively, as

$$\alpha(z) = \alpha_m(z) + \alpha_a(z), \tag{15}$$

$$p(\cos\Theta) = \frac{p_m(\cos\Theta)d\tau_m + p_a(\cos\Theta)d\tau_a}{d\tau_m + d\tau_a}, \tag{16}$$

$$\omega_0 = \frac{\omega_{0_m} d\tau_m + \omega_{0_a} d\tau_a}{d\tau_m + d\tau_a}. \tag{17}$$

Here $d\tau$ is the atmospheric optical thickness for an altitude element form z to $z + dz$.

3.3 Simulation and analysis

In the present simulation, we assume the following parameters: the solar zenith angle 37.75°, satellite observation zenith angle 0° (nadir looking), satellite altitude 850 km, satellite bandwidth 18100-18260 cm^{-1} (in wavelength, 0.5476-0.5525 μm), and solar irradiance 9.062 W/m^2. These values are in accordance with the parameters for NOAA AVHRR channel 1. The urban aerosol model is assumed for all the layers, with the single scattering albedo $\omega_{0a} = 0.9$ and the asymmetry parameter $g = 0.65$. The pixel size in the satellite image is 1 km × 1 km. For the maximum range of the adjacency effect calculation, we take $n = 15$ ($N = 31$) in eq. (14). For the vertical division of the atmosphere, we assume 51 layers in the altitude between 0 and 5 km, and 27 layers between 5 and 100 km. Details on the most essential parameters, namely the aerosol extinction profiles and the reflectance distribution of the ground surface, are explained below.

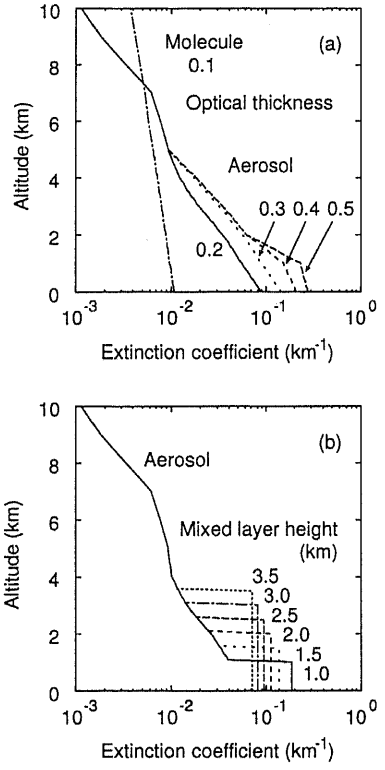

Figure 6: Aerosol and molecular extinction profiles used in the simulation. (a) Profiles based on the MODTRAN code. Here profiles with the aerosol optical thickness of 0.2 ∼ 0.5 are shown. (b) Profiles with variable mixed layer height. In this figure, the aerosol optical thickness is fixed at 0.3.

3.3.1 Aerosol extinction profile

A range of the aerosol optical thickness of τ_a = 0.18 to 0.50 (from the ground to the TOA) is considered here. Two kinds of extinction profiles are postulated as depicted in Fig. 6. The first type is model profiles used in the MODTRAN code. Figure 6 (a) shows such profiles for τ_a = 0.2, 0.3, 0.4, and 0.5. The other type is profiles in which a mixed layer with constant aerosol extinction exists up to a certain altitude, as illustrated in Fig. 6(b). In these profiles, the aerosol optical thickness is kept constant ($\tau_a = 0.3$ for the case of Fig. 6(b)) while the mixed layer height is varied as h_{ML} = 1.0, 1.5, ···, 3.0, and 3.5 km.

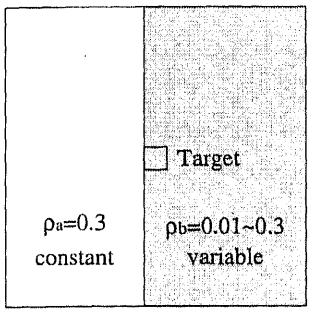

Two-reflectance surface

Figure 7: Flat and Lambertian surfaces with two reflectance values. ρ_a is fixed at 0.3, while ρ_b is varied between 0.01 and 0.3. The target area is placed on the border of the two surfaces, on the side of the surface with the variable reflectance.

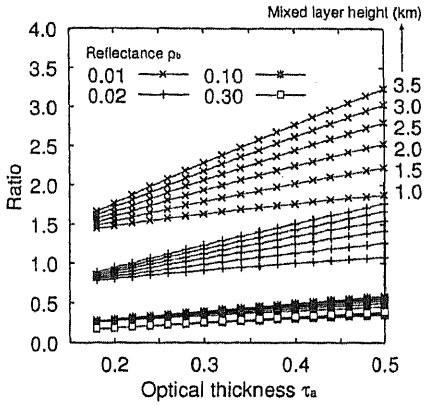

Figure 8: Adjacency effect relative to the ground-reflected irradiance. The curves show $r = E_{adj}/E_{gd}$ for various values of ρ_b and the mixed layer height h_{ML}.

3.3.2 Surface reflectance

In the present simulation, we adopt a situation with which the effect can be studied with the utmost clarity; namely we assume two (flat and Lambertian) surfaces with different reflectances (Fig. 7). As indicated in Fig. 7, the reflectance at the left side is fixed at $\rho_a = 0.3$, and that on the right side (ρ_b) is varied between 0.01 and 0.3. A target pixel is defined on the border of the two surfaces, on the side of the surface with the variable reflectance. We study the adjacency effect exerted on the "satellite image" of this target by changing the atmospheric as well as reflectivity conditions.

3.4 Results: Dependence on the surface reflectance

The influence of the surface reflectance is studied. Practically, it would be useful to give information on the ratio between the irradiances due to the adjacency effect and the direct ground reflection. Figure 8 shows the ratio $r = E_{adj}/E_{gd}$ as a function of the total aerosol optical thickness τ_a for various values of the surface reflectance ρ_b and mixed layer height h_{ML}. For the case of $\rho_b = 0.01$, the ratio is straightforwardly calculated from the E_{adj} and E_{gd}. It is found that the ratio r is larger for larger τ_a and larger h_{ML}. As the surface reflectance increases, r values are found to decrease, but exhibiting similar dependence on τ_a and h_{ML}. It is noteworthy that when ρ_b is small, even a small change of this value (*e.g.* from ρ_b =0.01 to 0.02) results in notable difference in the r values. When the surface reflectance is uniform (ρ_b = 0.3), the dependence on h_{ML} becomes minimal.

4. Conclusions

We have presented an algorithm in which only radiance components at the top of atmosphere are needed to calculate the reflectance of each pixel in satellite images. It has been shown that when the same atmospheric conditions are assumed for the construction of the test image and for the retrieval procedure, an accuracy of 1% is attained in the case of a visible image. The adjacency effect can easily be calculated on a pixel-by-pixel basis by means of our single scattering approximation. This calculation makes it possible to determine the range parameter N for each pixel. So far we have used aerosol models (i.e. wavelength dependence of the extinction) and aerosol vertical profiles provided in the MODTRAN source code. In this context, the data obtained with our multi-wavelength lidar will be quite beneficial to improve the actual atmospheric correction of the satellite images including Chiba area.

References

1) M. Minomura, H Kuze, and N. Takeuchi, Atmospheric correction of visible and near-infrared satellite data using radiance

components: an inproved treatment of adjacency effect, J. Remote Sensing Soci. Japan, in press.

2) R. Richter, A fast atmospheric correction algorithm applied to Landsat TM images, Int. J. Remote Sensing, **11**(1), pp.159-166, 1990.

3) T. Takashima and K. Masuda, The effect of land surface on the radiation emerging from the top of the atmosphere in the costal zone, J. Remote Sensing Soci. Japan, **18**(5), pp.3-13, 1997.

4) K. Thome, F. Palluconi, T. Takashima, and K. Masuda, Atmospheric correction of ASTER, IEEE Trans. Geosci. Remote Sensing, **36**(4), pp.1199-1211, 1998.